Acta Cryst. (1998). B**54**, 851–858

Net Intensities: Accuracy Improvement Through a Bayesian Perspective on the Measuring Strategy and Their Persistent Lack of Precision. An Illustration

A. T. H. Lenstra,[a]* B. Bracke,[a] B. van Dijk,[a]† S. Maes,[a] C. Vanhulle[a] and Herman O. Desseyn[b]

[a]*Department Structuurchemie, Antwerp University (UIA), Universiteitsplein 1, B-2610 Wilrijk, Belgium, and* [b]*Laboratorium Anorganische Scheikunde, Antwerp University (RUCA), Groenenborgerlaan 171, B-2020 Antwerpen, Belgium. E-mail: latifa@uia.ua.ac.be*

(*Received 26 June 1996; accepted 25 March 1998*)

Abstract

2,3-Diketopiperazine (2,3-piperazinedione), $C_4H_6N_2O_2$, crystallizes in the monoclinic space group $P2_1/c$ with a = 5.941 (3), b = 10.080 (3), c = 8.282 (2) Å, β = 95.87 (3)°, V = 493.4 (5) Å^3, Z = 4, D_x = 1.536 Mg m^{-3} and M_r = 114.1. The six-membered ring adopts a skew-boat conformation with Q = 0.467 (3) Å, θ = 64.6 (3)° and φ = 269.8 (4)°. The C_2 symmetry, which typifies the free molecule, is broken by the formation of two intermolecular N—H···O bonds involving only one of the C=O groups of the 2,3-diketopiperazine molecule. The intensity data typical for a time series are summarized in traditional statistics by $B = \sigma^2(B) = \Sigma B_i$ and $R = \sigma^2(R) = \Sigma R_i$, where B is the background and R the raw intensity. Exploitation of the same data using Bayesian methodology leads to similar values for B and R, but the variances for these signals are significantly smaller. This reduction in variance is dictated by the length N of the time series. With 25 observations in each *hkl* time series we arrive at variances that are 25% of their classical values. So, a measuring strategy in which a single observation with a slow scan at speed $1/N$ is preferred above a series of N observations at speed 1 produces the worst possible benefit within a fixed time frame. In complete contrast to our expectation, structure refinements reveal that that the standard deviation of an observation of unit weight, S, will converge towards its ideal unit value only when we decrease the accuracy of the data set. This unpleasant behaviour points to a serious discrepancy between accuracy and precision. Our reflection intensities are systematically wrong, because we underestimate the wavelength dispersion. On our CAD-4 equipment a sealed Mo tube and the standard graphite monochromator produce an incident beam with $\Delta\lambda/\lambda$ = 14%. As a consequence, the observed background intensities are not representative of the real background. The size of the background error depends on the nearby Bragg intensity. The magnitude of the signal pollution contaminating the local background is ~2% of the maximum Bragg intensity found at λ = 0.71 Å.

1. Introduction

2,3-Diketopiperazine is a cyclic oxamide, in which the oxamide unit is forced to adopt a *cis* configuration owing to the constraints of the ring system. This renders 2,3-diketopiperazine a useful model compound in the study of the *cis* secondary amide group (Lenstra *et al.*, 1998).

Its solid-state structure is analyzed in §2 on the basis of X-ray diffraction. The small size of the structure makes it very attractive to explore variations in the measuring strategy. These variations were designed to improve the accuracy of Bragg intensities.

In two previous papers (Lenstra, Geise & Vanhouteghem 1991; Lenstra, Verbruggen *et al.*, 1991) we have reported on the possibilities of data improvement *via* a structured background analysis. Theoretically the background is a simple function of the Bragg angle θ. This allowed us to summarize all the observed backgrounds over a certain θ interval in a local background distribution $P(B)$. The observed raw intensity R contains the net intensity I and the local background B. Since I and B are unrelated, we have $P(R) = P(I)P(B)$ with $\sigma^2(R) = \sigma^2(I) + \sigma^2(B)$. Combining the measurement R, which characterizes $P(R)$, with the local background distribution $P(B)$ we arrive at a net intensity *via* $P(I) = P(R)/P(B)$, which results in $\sigma^2(I) \simeq I$. Therefore, a background model reduces the background to a 'non-event' in error analysis. In this way small intensities gain a magnitude in accuracy.

To decrease the error margins typical for larger intensities ($R \simeq I$) we need to follow a different strategy. For clarity we confine ourselves to a fixed time measurement. Our current working practice favors a single slow scan. The alternative strategy is to spend the same time creating a time series of equivalent measurements, all observed at the maximum scan speed of the diffractometer. Traditional statistics point to an equivalence between these two strategies. However, as shown in §3, this equivalence breaks down in a Bayesian

† ERASMUS exchange student from the Department of Crystal and Structural Chemistry, State University of Utrecht, Padualaan 8, The Netherlands.

perspective, which leads to significantly smaller error margins.

In §4 we see that a systematic increase in the accuracy of the data set $\{I\}_H$ has only a marginal effect on R values. More disturbing is the behavior of S. It increases with increased data accuracy. Rather than converging to its 'ideal' unit value, S, which is defined as $\langle \Sigma \Delta I^2/\sigma^2(I) \rangle$, deviates more and more from unity. Consequently, the least-squares errors $\{\Delta I\}_H$ cease to reflect the random errors $\{\sigma(I)\}_H$ which are representative of the experiment performed.

This unexpected response of S to significant reductions in $\{\sigma(I)\}_H$ is discussed in §5. The data set $\{I_{obs}\}_H$ is shown to be accurate, but imprecise. The net intensities systematically underestimate the true intensity, because the incident X-ray beam is not really monochromatic. It is characterized by a wavelength dispersion of 14%. This value is typical for an incident beam produced by a sealed Mo tube combined with a standard pyrolytic graphite monochromator (mosaicity 0.4° full width at half height of the rocking curve). As a result of this large wavelength dispersion, the observed backgrounds are seriously polluted by a rest signal with size roughly equal to 2% of the nearby Bragg intensity observed at the θ position which coincides with λ(Mo $K\alpha$). The size of the error depends on θ and other factors. Therefore, errors induced by the wavelength dispersion influence both the scale factor and the displacement parameters. Since I_{net}/I_{true} decreases with θ, the lack of precision in $\{I_{net}\}_H$ leads to a systematic error, which causes the apparent displacement parameter B(X-ray) to overestimate the true atomic displacements.

It is well established that X-ray diffraction experiments produce larger displacement parameters than neutron diffraction (Craven & McMullan, 1979; Klebe *et al.*, 1984; Coppens *et al.*, 1984, oxalic acid project; Fuess, 1990). A valid explanation for this systematic discrepancy is still missing. We feel that the 14% wavelength dispersion, which affects X-ray data collection and which is subsequently ignored in the data analysis, is mainly responsible.

2. X-ray determination

A crystal of 0.20 × 0.25 × 0.15 mm was mounted on an Enraf–Nonius CAD-4 diffractometer. Cell dimensions were inferred from the angular setting of 25 reflections with $4 < \theta < 16°$ using graphite monochromated Mo radiation (λ = 0.71073 Å). 1015 reflections ($0 < h < 7$; $0 < k < 12$; $-9 < l < 9$) were measured up to a Bragg angle of 25° in an $\omega/2\theta$ scan mode. Three intensity control reflections were measured every 2 h. Their signals showed no significant intensity variations. No absorption correction (μ = 0.12 mm^{-1}) was applied. Systematic extinctions pointed at the space group $P2_1/c$. The structure was solved with *MULTAN* (Germain *et al.*, 1971). All H atoms were located in a difference electron density map. Full experimental details are given in Table 1.

Table 1. *Experimental details*

Crystal data	
Chemical formula	$C_4H_6N_2O_2$
Chemical formula weight	114.1
Cell setting	Monoclinic
Space group	$P2_1/c$
a (Å)	5.941 (3)
b (Å)	10.080 (3)
c (Å)	8.282 (2)
β (°)	95.87 (3)
V (Å^3)	493.4 (5)
Z	4
D_x (Mg m^{-3})	1.536
Radiation type	Mo $K\alpha$
Wavelength (Å)	0.71073
No. of reflections for cell parameters	25
θ range (°)	4–16
μ (mm^{-1})	0.12
Temperature (K)	293
Crystal form	Prism
Crystal size (mm)	0.25 × 0.20 × 0.15
Crystal color	Colorless
Data collection	
Diffractometer	Nonius CAD-4
Data collection method	$\omega/2\theta$ scans
Absorption correction	None
No. of measured reflections	1015
No. of independent reflections	1015
No. of observed reflections	457
Criterion for observed reflections	$I > 3\sigma(I)$
R_{int}	0.03
θ_{max} (°)	25
Range of h, k, l	$0 \rightarrow h \rightarrow 7$ $0 \rightarrow k \rightarrow 12$ $-9 \rightarrow l \rightarrow 9$
No. of standard reflections	3
Frequency of standard reflections	120 min
Intensity decay (%)	0
Refinement	
Refinement on	F
R	0.034
wR	0.037
No. of reflections used in refinement	457
No. of parameters used	97
H-atom treatment	All H-atom parameters refined
Weighting scheme	Counting statistics
$(\Delta/\sigma)_{max}$	0.05
$\lvert\Delta\rho\rvert_{max}$ (e Å^{-3})	0.25
Extinction correction	None
Source of atomic scattering factors	*International Tables for X-ray Crystallography* (1974, Vol. IV)

In the least-squares optimization (on $|F|$) of the structure model we used 457 intensities ($I > 3\sigma$) with weights based on counting statistics. Residuals converged at R = 0.034 and wR = 0.037. The maximum value for $|\Delta\rho|$ in the final difference Fourier was 0.25 e Å^{-3}. The maximum shift/error was 0.05. Final parameter values for x, y, z and B_{eq} are shown in Table 2. The atomic numbering scheme is illustrated in Fig. 1.

Table 2. *Fractional atomic coordinates and equivalent isotropic displacement parameters (Å²)*

$$B_{eq} = (4/3)[a^2\beta^{11} + b^2\beta^{22} + c^2\beta^{33} + (2ab\cos\gamma)\beta^{12} + (2ac\cos\beta)\beta^{13} + (2bc\cos\alpha)\beta^{23}].$$

	x	*y*	*z*	B_{eq}
O1	0.2785 (3)	0.0027 (2)	0.1096 (3)	3.28 (4)
O2	0.5621 (3)	0.1568 (2)	0.3128 (3)	4.08 (5)
N1	0.3552 (3)	0.3374 (2)	0.2296 (3)	2.89 (5)
C2	0.1642 (4)	0.3934 (3)	0.1291 (4)	2.98 (6)
C3	−0.0360 (5)	0.3046 (3)	0.1308 (4)	2.81 (6)
N4	0.0279 (3)	0.1705 (2)	0.0880 (3)	2.56 (5)
C5	0.2273 (4)	0.1182 (3)	0.1369 (3)	2.29 (5)
C6	0.3997 (4)	0.2073 (3)	0.2352 (2)	2.49 (6)
HN1	0.459 (4)	0.389 (3)	0.278 (3)	1.3 (6)†
HN4	−0.075 (4)	0.117 (3)	0.032 (3)	1.7 (6)†
H21	0.127 (4)	0.483 (3)	0.175 (3)	1.5 (6)†
H31	−0.155 (4)	0.333 (2)	0.048 (3)	0.2 (5)†
H22	0.203 (4)	0.407 (3)	0.019 (3)	1.0 (6)†
H32	−0.093 (4)	0.300 (3)	0.237 (3)	1.1 (6)†

† These atoms were refined isotropically.

Bond distances, valence angles and torsion angles are listed in Table 3. The six-membered ring contains two planar moieties, *viz.* C3—N4—C5—O1 and C2—N1—C6—O2, with a dihedral angle of 17° between them. The ring itself has a skew-boat conformation [ideal Cremer & Pople (1975) coordinates: θ = 67.5, φ = 270°]. The bond length C5—C6 is very long [1.532 (4) Å] for a Csp^2—Csp^2 distance, but is in keeping with the values in transoxamides such as oxamide (de Wit & Harkema, 1977) and oxalyldihydrazide (Bracke *et al.*, 1988; Quaeyhagens *et al.*, 1990). In our opinion this length indicates that the conjugation between the two π systems within the molecule is either absent or very weak.

The two intermolecular N—H···O bonds (Table 3) introduce an asymmetry in the 2,3-diketopiperazine molecule. Within a peptide moiety the C═O bond length increases by 0.011 Å for each hydrogen bond in which the O atom acts as an acceptor (Popelier *et al.*, 1991). Here the expected difference of 0.022 Å between C5—O1 and C6—O2 is matched by an experimental one of 0.016 (6) Å. This bond-length variation is compatible with that observed in acetamide. Here the C═O bond length is 1.220 (3) Å in the gas phase (Kitano & Kuchitsu, 1973), *i.e.* in the absence of hydrogen bonds, but in its *R*3*c* solid-state structure (Jeffrey *et al.*, 1980) with two hydrogen bonds per oxygen the C═O length is 1.250 (1) Å. 2,3-Diketopiperazine shows the same discrepancy within a single molecule in the solid state.

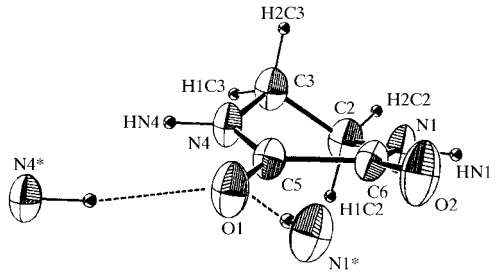

Fig. 1. 2,3-Diketopiperazine and its atomic numbering scheme. Ellipsoids at 50% probability are shown. The two hydrogen bonds accepted by each molecule are indicated.

Table 3. *Selected geometric parameters (Å, °)*

C5—O1	1.230 (4)	C3—N4	1.458 (4)
C6—O2	1.215 (4)	N1—HN1	0.87 (4)
C6—N1	1.338 (4)	N4—HN4	0.90 (4)
C5—N4	1.322 (4)	C2—H21	1.02 (3)
C5—C6	1.532 (4)	C2—H22	0.97 (3)
C2—C3	1.490 (4)	C3—H31	0.98 (3)
C2—N1	1.451 (4)	C3—H32	0.98 (3)
O1—C5—C6	119.2 (2)	N1—C6—C5	116.0 (2)
O1—C5—N4	123.5 (2)	N4—C5—C6	117.3 (3)
O2—C6—C5	119.1 (2)	C2—N1—C6	122.8 (3)
O2—C6—N1	124.9 (3)	C3—N4—C5	122.9 (3)
O1—C5—C6—O2	−15.4 (4)	C3—N4—C5—C6	−3.3 (4)
C3—N4—C5—O1	175.6 (2)	C5—C6—N1—C2	−3.8 (4)
C2—N1—C6—O2	177.1 (3)	C6—N1—C2—C3	38.6 (4)
O1—C5—C6—N1	165.4 (2)	N1—C2—C3—N4	−52.6 (3)
O2—C6—C5—N4	163.5 (2)	C2—C3—N4—C5	37.9 (4)
N4—C5—C6—N1	−15.6 (3)		

D—H···*A*	*D*—H	H···*A*	*D*—*A*	*D*—H···*A*
N1—HN1···O1^{i}	0.87 (3)	2.08 (3)	2.951	177 (3)
N4—HN4···O1^{ii}	0.90 (3)	2.01 (3)	2.906	174 (3)

Symmetry codes: (i) $-x, -y, -z$; (ii) $1-x, \frac{1}{2}+y, \frac{1}{2}-z$.

The same interactions are visible in the displacement parameters obtained from our X-ray model for O1 and O2. Since B_{eq}(C6) and B_{eq}(C5) are almost identical, the difference in ΔU of 0.010 (1) Å² in the mean-square displacements of O1 and O2 does not reflect an intramolecular phenomenon. It reveals a local anomaly induced by the N1—H···O1 and N4—H···O1 interactions restricting the mobility of O1. The hydrogen bonds have elongated C5═O1 and thus the force constant of the C═O stretching is lowered by a loss in bond strength. The intramolecular mobility of O1 is thus increased by the same elements that have restricted its overall mobility in the crystal lattice.

3. The benefit of a time series in data collection

Let us compare the results of two different schemes. First we observe a diffracted intensity in a single scan with a scan speed of 1/*N*. The observed integrated intensity is *R* counts with a counting statistical variance equal to *R*.

In the second analysis we measure the same reflection *N* times with a scan speed equal to 1. Each of these measurements results in integrated intensities C_i with a variance of C_i. In both experiments the total exposure time used to determine the intensity is identical. Therefore, both options lead to a similar result, *i.e.* $R \simeq \Sigma C_i$ and $\sigma^2(R) \simeq \Sigma\sigma^2(C_i)$. In practical work the slow

measurement is favored above a repeated measurement, because it requires only one single positioning command for the diffractometer setting.

The slow measurement produces a single observation of R counts. This value is indicative of the true intensity r. It is r we are really interested in. R and r are related *via*

$$P(r|R) = P(R|r)P(r). \quad (1)$$

The likelihood $P(R|r)$ is a counting statistical distribution is given by $\exp[-(R-r)^2/2r]$.

Let us now construct the prior $P(r)$. It follows from probability theory that there is 99.7% probability that R is unacceptable if $|(r-R)| > 3\sigma(r)$. Therefore, any r used to describe the true signal, which results in $|r-R| > 3\sigma(r)$, has to be regarded as an unsatisfactory proposition. The acceptable r values are thus situated between

$$r_{\min} = R - 3\sigma(r_{\min})$$
$$\text{and } r_{\max} = R + 3\sigma(r_{\max}).$$

In a counting statistical framework we have $\sigma^2(r_{\min}) = r_{\min}$ and $\sigma^2(r_{\max}) = r_{\max}$.

Given the observation R we obtain $P(r) = 0$ for any $r < r_{\min}$ and $r > r_{\max}$. To express our ignorance related to the true value of r, $P(r)$ is a uniform distribution in the intensity interval between $r_{\min}$ and $r_{\max}$.

Substitution of $P(R|r)$ and $P(r)$ in (1) yields

$$\langle r|R\rangle \simeq R \text{ and } \sigma^2(r|R) \simeq R.$$

In the absence of an 'informative prior' the real measurement dictates the final result.

Let us now re-examine the results C_i in the time series. One advantage of a series of N observations is obvious. Outliers, caused by multiple scattering or diffractometer instabilities, are easily detected and removed from our data set. This suffices to illustrate that the end result in this reconstruction of the underlying signal is more robust in spite of the fact that the final result appears to be identical to the slow measurement.

To estimate the added value is not very complicated. Suppose that our time series is not contaminated by an outlier. The two extreme values in our C_i series are $C_{\max}$ and $C_{\min}$. The ideal value of the signal is c. $C_{\max}$ constrains this ideal signal c to values between $C_{\max} - 3\sigma(c_{\min})$ and $C_{\max} + 3\sigma(c_{\max})$. $C_{\min}$ also limits the acceptable c values to values between $C_{\min} - 3\sigma(c'_{\min})$ and $C_{\min} + 3\sigma(c'_{\max})$. Therefore, the two extreme C_i observations limit the range of acceptable c values between $C_{\min} + 3\sigma(c'_{\max})$ and $C_{\max} - 3\sigma(c_{\min})$. This is illustrated in Fig. 2, which also shows the prior distribution $P(c)$.

In a time series of 30 elements the average difference between $C_{\max}$ and $C_{\min}$ is ~4 e.s.d.'s. Consequently, the function interval, in which $P(c) \neq 0$, has a width of $2\langle C\rangle^{1/2}$. This distribution width is small compared with the value of $6\langle C\rangle^{1/2}$ connected to the counting statistical distribution $P(C_i|c)$. So $P(c)$ is an informative prior.

Substitution of $P(C_i|c)$ and $P(c)$ in (1) produces the posterior distribution $P(c|C_i)$, which enables us to enumerate $\langle c|C_i\rangle$ and $\sigma^2(c|C_i)$. A direct summation over all i posterior moments then reproduces the signal with a value $\sim R$ and its variance σ^2. In the single measurement strategy $\sigma^2 \simeq R$; in our time series strategy we obtain a much smaller value, *viz.* $\sigma^2 \simeq R/10$.

The global estimate of the resulting variance is easily obtained. The prior $P(c)$ is nonzero in a 2σ (counting statistics) interval. To simplify the algebraic expression we approximate $P(c)$ *via* a normal distribution. Then, $6\sigma(\text{prior}) \simeq 2\sigma(\text{counting statistics})$ and thus $\sigma^2(\text{prior}) = \sigma^2(\text{counting statistics})/10$. Since $P(c)$ is more informative than the counting distribution $P(C_i|c)$, the posterior moments to be obtained from (1) are

$$\langle c|C_i\rangle \simeq \langle C\rangle \text{ and } \sigma^2\langle c|C_i\rangle \simeq \sigma^2(\text{prior}) = C/10.$$

We decided to use 2,3-diketopiperazine for a comparison between the traditional statistical approach and alternative logic, in which the Bayesian rules allow one to take full advantage of the sociological composition of the available time series.

4. Refinement and data accuracy

Every reflection up to $\theta = 25°$ was measured 25 times at slightly different azimuth angles ($0 \leq \psi \leq 24°$ in steps of 1°) using the maximum diffractometer speed in each individual scan. In view of the crystal size ($0.20 \times 0.25 \times 0.15$ mm) and the low value for μ ($0.12\ \text{mm}^{-1}$), the changes in azimuth angle do not introduce a significant variation in intensities caused by absorption.

We checked the internal consistency of our intensity measurements. For this purpose we created five data sets, in which the original 25 measurements per reflection were combined over ψ intervals of 5°. Mixing these five independent data sets of 1015 reflections each we calculated a merging R of 0.03.

We started our analysis with the classical recipe of summing equivalent data. χ^2 was used to detect possible outliers in each time series of background and raw intensity. If present, that observation was omitted from the data summation. Net intensities were calculated following the classical background–peak–background procedure.

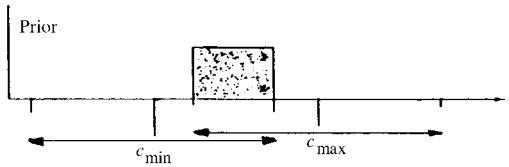

Fig. 2. The construction of an informative prior from $C_{\min}$ and $C_{\max}$, which are the two extremes in a time series of identical measurements.

Table 4. *Least-squares and Fourier evidence ($\Delta\rho_{max}$, e Å^{-3}) as a function of the accuracy characteristic for the data set*

Here accuracy depends on the length n of a time series of equivalent measurements available for *hkl*. The number of refined parameters was 97 in all calculations.

	2,3-Diketopiperazine					Lithium hydrogen maleate dihydrate				
n	R	wR	N_{obs}	S	$\Delta\rho_{max}$	R	wR	N_{obs}	S	$\Delta\rho_{max}$
1	0.053	0.058	279	1.416	0.34	0.035	0.047	1368	1.543	0.37
2	0.049	0.054	335	1.406	0.34	0.034	0.046	1462	1.644	0.38
4	0.047	0.055	400	1.502	0.27	0.033	0.047	1555	1.761	0.40
9	0.042	0.056	466	1.667	0.26	0.032	0.048	1636	1.901	0.43
16	0.042	0.059	521	1.849	0.28	0.032	0.052	1702	2.140	0.45
25	0.047	0.054	553	1.942	0.25	0.033	0.056	1769	2.356	0.46
Bayes	0.062	0.075	647	2.745	0.34					

We constructed different data sets for 2,3-diketopiperazine by combining n elements per reflection **H** from the time series of 25 individual observations. The structure of 2,3-diketopiperazine was subsequently optimized using that particular data set. The least-squares results are summarized in Table 4 for the data sets with $n = 1, 2, 4, 9, 16$ and 25. Final parameter values in each analysis did not deviate more than 3 e.s.d.'s from the values presented in Table 2.

Combining n individual measurements into a single result increases the accuracy of the latter. Its standard error follows $n^{-1/2}$. This explains the increase in N_{obs}, the number of observations with $I > 3\sigma(I)$, as a function of n. R values, weighted or unweighted, do not follow the pattern of the improved accuracy per data set on offer. Increasing the data accuracy by a factor of five causes R to shift marginally from 0.053 to 0.047. Most disturbing, however, is the behavior of $S = \chi^2/N_{obs} = \Sigma[\Delta I/\sigma(I)]^2/N_{obs}$. S compares the randomized least-squares errors $\{\Delta I\}_H$ with the random errors $\{\sigma(I)\}_H$ typical for our experiment. The fact that as S deviates more from its ideal unit value the more accurate the data set becomes tells us that ΔI(least-squares) is out of step with $\sigma(I)$(experiment). To be certain we double-checked this surprising S trend. In this experiment we used the more rigid structure of lithium hydrogen maleate dihydrate (Popelier *et al.*, 1989) as a reference compound. The results (see Table 4) are practically identical to those obtained for 2,3-diketopiperazine.

A Bayesian treatment of the diffractometer data yields posterior standard deviations σ', which are smaller than the counting statistical values σ. We now obtained 647 reflections with $I > 3\sigma'(I)$. Structure optimization converged at $R = 0.061$ and $wR = 0.075$.† Again the shifts in model parameters were insignificant (maximum shift/error = 2.5). The maximum noise level in the final difference electron density was -0.3 e Å^{-3}.

† The selective addition of small intensities to the data used in the least-squares optimization hardly influences $\Sigma|F_o|$. $\Sigma|\Delta|$, however, increases in line with the number of contributors. This is reflected in the variation of the observed R values.

$\sigma' < \sigma$ and $I' \simeq I$ summarizes concisely the consequences of the two strategies; this explains the 15% increase of data exploited in the least-squares analysis. These extra reflections are in fact the bulk of the intensities between 1.5σ and 3σ in the traditional data set. This indicates that $3\sigma' \simeq 1.5\sigma$ and thus the Bayesian logic leads to posterior values for the variance which are 25% of the traditional counting statistical value.

This overall reduction in variance matches nicely with our crude, but optimistic, estimate of σ^2(posterior) $\simeq 0.1 \times \sigma^2$(counting statistics); see §3.

In our opinion this study demonstrates clearly the potential gain in accuracy which is attainable within the framework of fixed time measurements. All we have to do is replace a slow scan by a series of N measurements at high speed. The greater the N value, the higher the final accuracy because N determines the average distance between C_{min} and C_{max}.

An increase in experimental accuracy should, at least in principle, lead to a decrease in the e.s.d.'s on the refined model parameters. We expect a reduction in σ(model), because (*a*) σ(model) is proportional to σ(observation) and (*b*) σ(model) is inversely proportional to $N_{obs}^{1/2}$, where N_{obs} is the number of observations included in the least-squares analysis.

In our model optimizations, σ(model) is only in keeping with $(N_{obs})^{-1/2}$. Therefore, σ(model) behaves as if it were independent from the (significant) variations on offer in σ(observation). The absence of a detectable correlation between σ(model) and σ(observation) is logical, when the real quality of I_{obs} is dictated by a systematic error exceeding the random error characterizing the experiment.

If true, this is a painful conclusion. It would seriously undermine *e.g.* maximum entropy methods as a tool to produce an improved set of Δ's *via* flat difference Fourier maps.

The absence of a significant correlation between ΔI(least-squares) and $\sigma(I)$(experiment) is underlined by the trend in S values (see Table 4). Rather than converging to its ideal unit value with increasing accuracy in the data set, we observe exactly the reverse. This

also suggests that the precision of I_{obs} is quite different from its accuracy.

5. Precision *versus* accuracy

The quality of a structure analysis depends on the efficiency of the selected model parameters and/or on the reliability of the initial data. It is clear from Table 4 that the R values do not follow the accuracy pattern characteristic for the data set at hand. Therefore, the model parameters **r** and β might be too crude to exploit this accuracy. This inefficiency is, in our view, connected to our least-squares approach, in which ρ(atom) is spherically symmetric and in which an harmonic potential governs the atomic displacements. These limitations of the model can be tackled *e.g.* by a multipole refinement, which is known to lead to a significant decrease in R values. Therefore, we feel that model shortcomings cannot be ruled out as a potential source of confusion.

The observed behavior of S poses a serious challenge. The discrepancy between the least-squares errors $\{\Delta I\}_H$ and the experimental errors $\{\sigma(I)\}_H$ grows with increased accuracy of $\{I_{obs}\}_H$. This unpleasant trend points to a lack of precision in $\{I_{obs}\}$ generated by a systematic error. Randomization of this error in a least-squares calculation is then responsible for the observed pattern in S values. We believe we have identified the systematic error which reduces the quality of $\{I_{obs}\}_H$, namely a serious misjudgement of the wavelength dispersion characteristic for the incident X-ray beam.

To analyze the wavelength distribution typical for the incident beam we installed an Si crystal (0.5 × 0.5 × 0.5 mm) on our diffractometer. The incident beam was produced by an Mo tube in combination with a graphite monochromator [net plane (002); mosaicity 0.4° full width at half height in the rocking curve]. The mosaicity of the Si crystal was extremely small (0.005°), which helped to minimize wavelength smearing in its reflection profile. The Si(12 0 0) reflection with θ = 51.8° was used in our wavelength-dispersive analysis. Scans were made using the $\omega/2\theta$ scan mode over an angular range in ω (or θ) of 21°. The observed profiles were dumped in 96 channels.

In our first series of measurements we used our CAD-4 diffractometer. The incident X-ray beam was produced by a sealed Mo tube (focal spot 0.4 × 8.0 mm; take-off angle ~6°) installed upon our FR-586 generator with a setting of 20 mA and 50 kV. The results are depicted in Fig. 3. Using 187 individual profile dumps we calculated the average signal μ_i and its spread s_i^2 per channel i. At the reflection maximum, s^2 is significantly larger than μ. This deviation from counting statistics is indicative of positional and electrical uncertainties. Positional errors were estimated by calculating the spread for the center of gravity in the 189 individual profiles. The s.u. on the gravity center was found to be 0.09 channel or 0.02° in ω. The electrical stability was estimated by comparing the integrated intensities per profile scan. Assuming s^2(observed) = σ^2(counting statistics) + $(pI)^2$, we inferred an electrical error p of 0.01. As can be seen in Fig. 3, the Si(12 0 0) reflection begins at λ = 0.68 Å and ends at λ = 0.79 Å. Therefore, the wavelength dispersion $\Delta\lambda/\lambda$ typical for the incident beam is 0.14.

We repeated this experiment on our recently purchased Mach-3 diffractometer installed on a rotating Mo anode (focal spot 0.3 × 3 mm) coupled to an FR-591 generator. On this combination the random error on the center of gravity was 0.02 channel (0.004°), whereas the electrical error decreased to p = 0.004. Both errors are practically independent of the tube current, which we varied from 10 to 50 mA. The results of the Si(12 0 0) measurements are shown in Fig. 4. Counting statistical errors hold everywhere, except in the profile maximum. Here s^2/μ increases with increasing tube current and thus with increasing X-ray intensity. The increase in s^2/μ

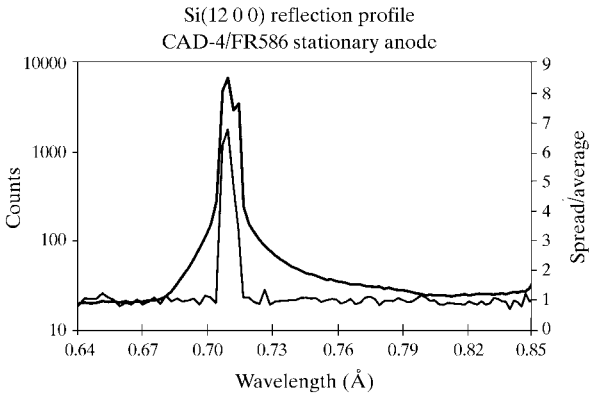

Fig. 3. The averaged Si(12 0 0) profile (thick curve) and its reproducibility represented by s^2/μ. Minimum and maximum wavelengths in the Si(12 0 0) profile are 0.68 and 0.79 Å.

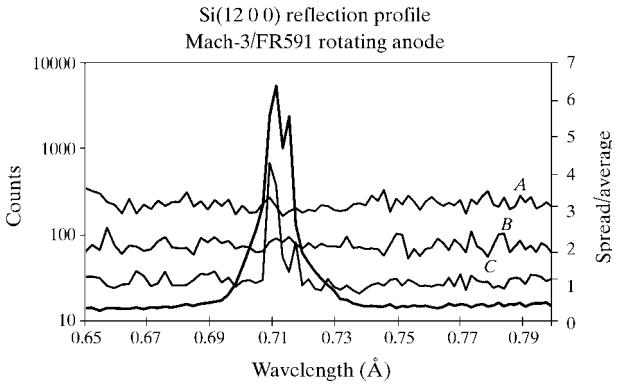

Fig. 4. The averaged Si(12 0 0) profile (thick curve) from the same Si specimen as in Fig. 3 observed on a rotating anode device operated 50 kV, 20 mA. *A*, *B* and *C* represent s^2/μ for measurements at tube currents of 10, 20 and 50 mA, respectively. For clarity their unit value base line is shifted to 2.0 for *B* and 3.0 for *A*. Observed (12 0 0) wavelength limits are 0.69 and 0.75 Å.

at the reflection maximum is in keeping with an electrical error fixed at 0.4%. In this experiment we find a reflection starting at $\lambda = 0.69$ Å and fading at $\lambda \simeq 0.75$ Å. Therefore, this time we have a wavelength dispersion of 0.09.

The profile scans with CAD-4 and Mach-3 equipment are both reproducible. The results are, however, quite different. This is indicated in Fig. 5 *via* the ratio between the two measurements. This ratio is far from constant. A detailed analysis of the wavelength dispersion will be presented in a forthcoming paper. Here it suffices to link the difference in $\Delta\lambda/\lambda$ between the stationary and rotating anode devices to the main difference in X-ray optics, which is the separation between the graphite monochromator and the silicon analyzer. This distance is 136 mm for the sealed tube/CAD-4 combination and it increases to 230 mm on the rotating anode/Mach-3 apparatus. In Fig. 6 we give a simplified model linking crystal size and monochromator–crystal separation to a $\Delta\theta$ variation. From Bragg's law $\Delta\theta$ is easily translated in $\Delta\lambda$. Since $\Delta\theta$ is small, we have $\tan\Delta\theta \simeq \Delta\theta$. A reduction in $\Delta\theta$ by 40% through a selective increase in the monochromator–crystal distance then leads to the observed shift in $\Delta\lambda/\lambda$ from 0.14 to 0.09.

The general expression for the scan angle to be used in data collection is given by $c = 1.5(a + b\tan\theta)$. For the 2,3-diketopiperazine measurement on our sealed tube/CAD-4 equipment we used $a = 1.2$ and $b = 0.7°$. Theoretically b is dictated by the wavelength dispersion *via* $b = (\Delta\lambda/\lambda)(360/2\pi)$. Therefore, the correct value for b, given $\Delta\lambda/\lambda = 0.14$, ought to be 8°.

However, a data collection with $c = 1.5(a + 8\tan\theta)$ is impossible, because very soon c becomes larger than the θ separation between adjacent lattice points. This prohibits the intensity measurement of individual reflections. Forcing a measurement, as we did, with $b = 0.7°$ turns the background into a very poor estimator of the real background. For example, the high θ background is seriously polluted by a rest signal from the λ tail of the preceeding reflection. This error is roughly 2% of the maximum intensity at $\lambda = 0.71$ Å. Consequently, the background–peak–background reconstructed intensity I_{net} systematically underestimates the true intensity I_{true}. Let us now introduce Δ, defined as $\Delta \equiv I_{net}/I_{true}$. Then Δ decreases with increasing θ. When we move from low-order intensities towards higher-order data the background is sampled closer (in θ and thus in λ) to the central reflection maximum at $\lambda = 0.71$ Å. This increases the signal contribution, which is superimposed on the real background, at the observation point. As can be seen in Table 4, S from lithium hydrogen maleate is always larger than S from 2,3-diketopiperazine. This systematic difference is, in our opinion, the logical consequence of the data collection parameter b. In 2,3-diketopiperazine we used $b = 0.7°$, whereas in the lithium compound we used $b = 0.6°$.

The only model parameter able to absorb Δ is the temperature factor. Since I_{net} decreases faster with θ than I_{true}, β(X-ray) overestimates the real atomic displacements. In elastic neutron scattering the distance between monochromator and crystal is roughly a magnitude larger than in our X-ray environment. Improving $\Delta\theta$ by a magnitude leads to an estimated wavelength dispersion of 0.02. In that framework the background observations are practically free of the intensity bias produced by the nearby signal (s) and thus B(neutron) is a much better estimator for the atomic displacements in the crystal than B(X-ray).

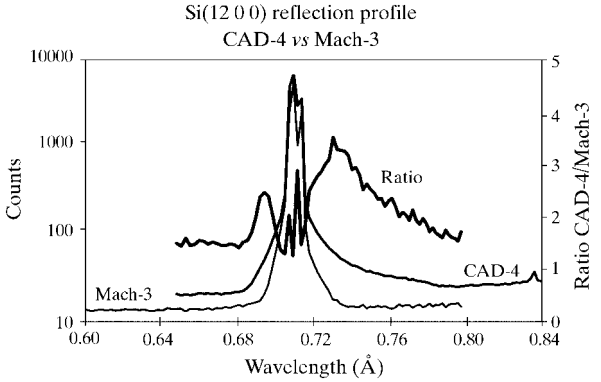

Fig. 5. The equipment-related profile differences are clearly visible *via* the intensity ratio R, which is far from a constant.

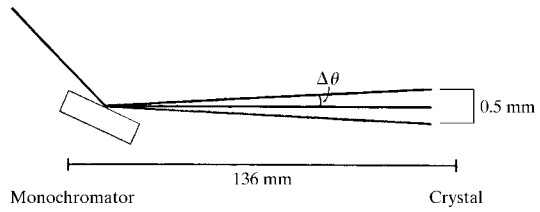

Fig. 6. $\Delta\theta/\theta$ (monochromator) determines the wavelength dispersion $\Delta\lambda/\lambda$. As shown, $\Delta\theta$ depends for a fixed crystal on the distance between the monochromator and the crystal to be analyzed.

References

Bracke, B., Lenstra, A. T. H. & Geise, H. J. (1988). *Z. Kristallogr.* **185**, 198.

Coppens, P., Dam, J., Harkema, S., Feil, D., Feld, R., Lehman, M., Goddard, R., Krüger, C., Hellner, E., Johansen, H., Larsen, F., Koetzle, T., McMullan, R., Maslen, E. & Stevens, E. (1984). *Acta Cryst.* A**40**, 184–195.

Craven, B. M. & McMullan, R. K. (1979). *Acta Cryst.* B**25**, 934–945.

Cremer, D. & Pople, J. A. (1975). *J. Am. Chem. Soc.* **97**, 1354–1358.

Fuess, H. (1990). *The Use of Neutron Diffraction in Charge Density Analysis*. NATO Summer School Course, San Feliu, Spain.

Germain, G., Main, P. & Woolfson, M. M. (1971). *Acta Cryst.* A**27**, 368–372.

Jeffrey, G. A., Ruble, J. R., McMullan, R. K., De Frees, D. J., Binkely, J. S. & Pople, J. A. (1980). *Acta Cryst.* B**36**, 2292–2299.

Kitano, M. & Kuchitsu, K. (1973). *Bull. Chem. Soc. Jpn*, **46**, 3048–3051.

Klebe, G., Bats, J. W. & Fuess, H. (1984). *J. Am. Chem. Soc.* **106**, 5205–5208.

Lenstra, A. T. H., Bracke, B., van Dijk, B., Maes, S., Van Alsenoy, C., Desseyn, H. O. & Perlepes, S. P. (1998). *Acta Cryst.* B**54**, 859–865.

Lenstra, A. T. H., Geise, H. J. & Vanhouteghem, F. (1991). *Acta Cryst.* A**47**, 597–604.

Lenstra, A. T. H., Verbruggen, M., Bracke, B., Vanhouteghem, F., Reyniers, F. & Borremans, F. (1991). *Acta Cryst.* B**47**, 92–97.

Popelier, P., Lenstra, A. T. H. & Geise, H. J. (1989). *Acta Cryst.* C**45**, 1024–1028.

Popelier, P., Lenstra, A. T. H., Van Alsenoy, C. & Geise, H. J. (1991). *Struct. Chem.* **2**, 3–9.

Quaeyhagens, F., Desseyn, H. O., Bracke, B. & Lenstra, A. T. H. (1990). *J. Mol. Struct.* **238**, 139–157.

Wit, G. de & Harkema, S. (1977). *Acta Cryst.* B**33**, 2367–2372.